Acta Geodyn. Geomater., Vol. 22, No. 1 (217), 105–120, 2025
DOI: 10.13168/AGG.2025.0008
journal homepage: https://www.irsm.cas.cz/acta

ORIGINAL PAPER

INTEGRATED PETROGRAPHIC, GEOCHEMICAL, AND MECHANICAL EVALUATION OF DIORITE ROCKS FOR SUSTAINABLE AGGREGATE USAGE: A CASE STUDY FROM ZARDALI BANDA AREA, NORTHERN PAKISTAN

Rehan KHAN [1], Syed Mamoon SIYAR [2], Abbas Ali NASEEM [1,*], Farhat ULLAH [1], Muhammad BILAL [3], Matloob HUSSAIN [1], Muhammad Atif BILAL[4,*] and Muhammad SHAHAB [5]

[1] *Department of Earth Sciences, Quaid-i-Azam University, Islamabad 45320, Pakistan*
[2] *Department of Geology, University of Malakand, Chakdara 18800, Pakistan*
[3] *School of Earth, Atmosphere and Life Sciences, University of Wollongong, Australia*
[4] *College of Geoexploration Science & Technology, Jilin University, Changchun 130061, China*
[5] *Abdullah Alrushaid Chair for Earth Science Remote Sensing Research, Geology and Geophysics Department, King Saud University, 2455, Riyadh 11451, Saudi Arabia*

**Corresponding author's e-mail:* abbasali@qau.edu.pk; bilal6517@mails.jlu.edu.cn

ARTICLE INFO

Article history:
Received 24 November 2024
Accepted 24 March 2025
Available online 5 April 2025

Keywords:
Diorite
Petrography
Physico-mechanical
Geochemical Analysis

ABSTRACT

The well-exposed outcrop of ZardAli Banda Diorite has been studied for its petrography, geochemistry, and physico-mechanical properties. The field investigations and petrographic observations indicate the primary composition of dark grey coarse-grained diorite is plagioclase, quartz, alkali feldspar (orthoclase), hornblende, clinopyroxene, orthopyroxene, and biotite, with a sufficient amount of sericite and traces of olivine. The geochemical signatures show the intermediate nature with SiO_2 percentages ranging from 56.63 % to 59.03 %, followed by Al_2O_3 composition ranges from 21.76 % to 24.01 %, CaO 8.2 % to 9.2 %, Fe_2O_3 6.04 % to 6.86 %, Na_2O 2.15 % to 3.67 %, TiO_2 0.37 % to 0.77 %, K_2O 0.61 % to 0.77 % and P_2O_5 0 %, respectively. The physico-mechanical tests, conducted according to ASTM standards, yielded average results of 2.832 gm/cm^3 for specific gravity, 0.627 % for absorption, 4.497 % for flakiness index, 6.527 % for elongation index, 12.58 % for Los Angeles Abrasion value, 3.357 % for soundness, 36.914 MPa and 6.151 MPa for UCS and UTS, respectively. These analyses are within the potential limit of ASTM to use as a successful aggregate. The UCS and UTS values fall in the medium-strong category. The impact of geochemical trends on physico-mechanical analyses reveals that variation in major oxides influences mineral crystallization, affecting strength, durability, and aggregate suitability, with an inverse relationship between SiO_2 and Fe_2O_3 enhancing compressive strength while CaO contributes to higher density and reduced absorption. The overall ASTM results of the ZardAli Banda Diorite suggest that these rocks can be used as an aggregate for heavy construction works (CPEC developmental scheme), road materials (Dir-Chitral Expressway), dams, and other construction projects.

1. INTRODUCTION

Igneous rocks are widely used materials in construction because of their extensive exposure, availability, pore spaces, and mineralogical composition, which make them ideal materials for roads, tunnels, bridges, and many other construction projects (Varghese, 2011). The igneous rocks are commonly used for dimension stones or aggregate materials (Strzałkowski et al., 2021). In Northern Pakistan, igneous rocks are closely associated with the Kohistan Island Arc, a region characterized by complex stratigraphy of ultramafic units to volcano-sedimentary units (Petterson, 2019). The Kohistan Island Arc is one of the largest intraoceanic subduction zones, covering a 30000 sq. km area. This intra-oceanic arc was formed due to the India-Asia collision-related tectonics (Zafar et al., 2019b, 2025; Nakazawa et al., 2020). This region is a remarkable natural laboratory containing certain geological units. The most prominent and basic units are the Kohistan Batholith and Kamila Amphibolite (Zafar et al., 2023). The Kamila Amphibolite stretches from the Nanga Parbat Haramosh syntaxes to Afghanistan, is well exposed at Lower Dir, and contains the lithology of diorite, gabbronorite, amphibolite, and felsic rocks (Jan et al., 1990).

The geological units of the Kohistan Island Arc are widely utilized in construction because of their mineralogical composition, durability, and availability. Previous studies include the physico-mechanical analysis of gabbronorite of Kamila Amphibolite in the Khagram-Razagram area of Lower Dir by Sajid et al. (2009) and the mineralogical and aggregate studies of the River Panjkora and Kunai River by Rahman et al. (2022). Additionally, the feasibility of using metasediments as coarse aggregate at Chakdara has been evaluated by Muhammad et al. (2022). Moreover, granitioids at

Cite this article as: Khan R, Siyar S M, Naseem AA, Ullah F, Bilal M, Hussain M, Bilal MA, Shahab M: Integrated petrographic, geochemical and mechanical evaluation of diorite rocks for sustainable aggregate usage: A case study from Zardali Banda Area, Northern Pakistan. Acta Geodyn. Geomater., 22, No. 1 (217), 105–120, 2025. DOI: 10.13168/AGG.2025.0008

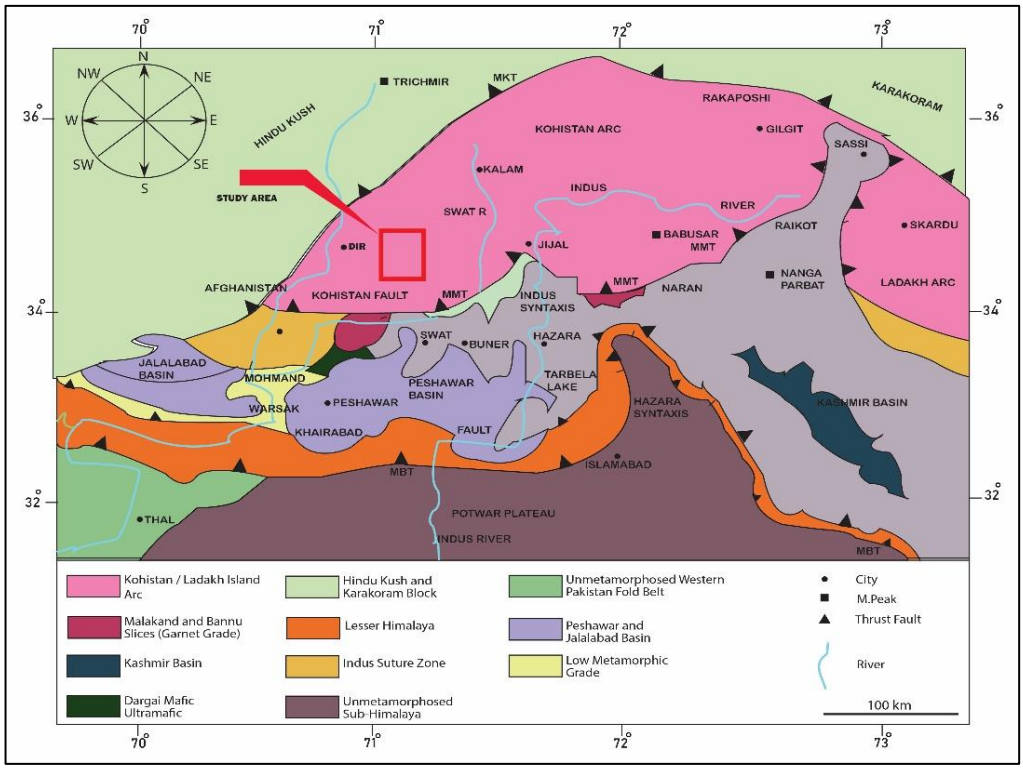

Fig. 1 Geological map of North-Western Himalayas, showing study area marked by red rectangle (Modified after Ahmad et al. (2003)).

a global scale were investigated to understand the magmatic sources, tectonic histories, and aggregate evaluation (Teymen, 2019; Zafar et al., 2019a, 2019b, 2020a; Rehman et al., 2021). However, there is limited research integrating petrographic, geochemical, and mechanical evaluations of diorite rocks from the Kamila Amphibolite. The existing studies primarily focus on the tectonic evolution and general geology of the Kamila Amphibolite, neglecting detailed assessments of diorite suitability for construction purposes. There is a lack of integrated research combining petrographic, geochemical content, and physio-mechanical analyses to comprehensively assess the construction potential of these rocks. Additionally, limited attention has been given to connecting the geological characteristics of Northern Pakistan's intermediate igneous rocks with their practical applications in large-scale infrastructure projects such as CPEC developmental schemes. These gaps underscore the need for a region-specific study to evaluate the suitability of ZardAli Banda Diorite exposed along Grand Trunk Mayar Road at 34°54′32″N to 71°36′10″E, 34°54′42″N to 71°36′39″E. This study aims to integrate petrographic, geochemical, and physio-mechanical analyses to assess the suitability of these rocks as sustainable construction materials for widespread infrastructure development.

2. GEOLOGY AND TECTONICS

The Kohistan Island Arc is the most complete intraoceanic subduction that stretches from the northward Ladakh Arc to the eastward Afghanistan (Khan et al., 2009). The Kohistan Island Arc collided with the Eurasian Plate at the north margin and developed the Andean type of orogeny (Richards, 2015). The south margin of the Kohistan Island Arc collided with the Indian Plate, and as a result, the consumption of the Neo-Tethys oceans beneath the Kohistan Island Arc and the Eurasian Plate (Gibbons et al., 2015). The Kohistan Island Arc is divided from the Ladakh Arc through the Nanga Parbat syntaxes and sandwiched between the Main Mantle Thrust at the south and the Main Karakorum Thrust to the north (Searle., 2019). This complex geological heritage covers a 30000 km^2 area and contains several stratigraphic lithologies ranging from ultramafic rocks to volcano-sedimentary units (Ullah et al., 2020a; Ullah et al., 2020b). The prominent stratigraphic units of the Kohistan Island Arc are the Jijal Complex, Sapat and Tora Tiga Complexes, Kamila Amphibolites, Chilas Complex, Kohistan Batholith, Chalt volcanic group, and Yasin Group metasediments (Ullah et al., 2023; Ullah et al., 2022; Zafar et al., 2020b, 2021, 2023, 2024). The Kamila Amphibolite is one of the most basic units of the Kohistan Island arc having a length of 350 km and maximum width up to 50 km extends from the western flanks of Nanga Parbat Hramosh syntaxes to Swat, Dir, and Afghanistan (Jan, 1990). The Kamila Amphibolites contain metavolcanics and metaplutonics that make up the majority of the Kamila domain, which stretches roughly 250 km from east to west. The metaplutonic rocks are composed of gabbros, norites, and diorites, whereas the metavolcanic rocks are primarily composed of basalts and basaltic andesites (Eyal et al.,

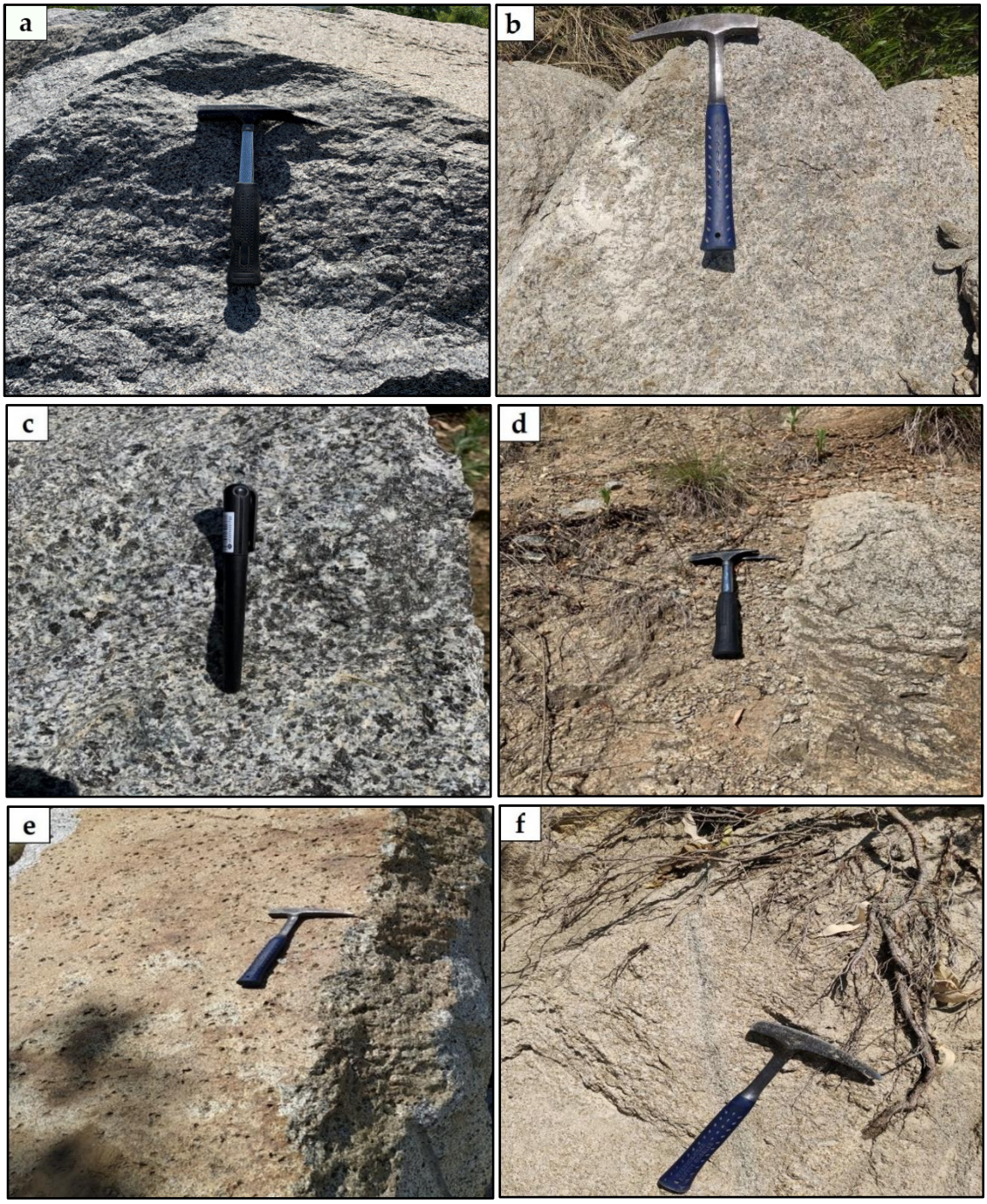

Fig. 2 Outcrop features (**a**) Weathered surface (**b**) Fresh surafce (**c**) Fresh surface having concentration of hornblende (**d**) Diorite having quartz, feldspars veins (**e**) Diorite having dissolution of mica (**f**) Diorite having thread vein.

2019). The geochemical trend of the metaplutonic rocks is calc-alkaline to tholeiitic (Kausar et al., 2004). The age of the Kamila Amphibolite through hornblende–Ar–Ar is 83 Ma, but zircon–U–Pb geochronology generated an estimated 110–75 Ma (Treloar et al., 1989). A range of exposed plutonic units along the Indus River between Dasu and Patan, including Sarangar-gabbro, diorite, and granite within the Kamila unit, have produced the U-Pb age spectrum between 91.8 and 98.9 Ma (Herburger, 2004).

3. MATERIALS AND METHODS

3.1. FIELD OBSERVATIONS

The ZardAli Banda Diorite is medium to coarse-grained intrusive bodies, predominantly exhibiting a dark grey color on weathered surfaces and brownish on fresh surfaces. These diorite rocks are characterized by alternating shear and compacted zones. These compacted zones display reduced fracture density and enhanced cohesion wheres the sheared zones are distinguished with moderate to intensive weathering and dissolution of mica, as illustrated in Figure 2. The

Table 1 Table showing the minerals visualized estimated percentage of ZardAli Diorite.

Sample	Plg %	Qz %	AF %	Hbl %	Cpx %	Opx %	Bt %	Ol %	Sr %
MG1	68	02	10	5	7	1	5	-	2
MG2	69	1.5	2	6	10	4	6	-	1.5
MG3	74	1	2	3	15	-	4	-	1
MG4	70	2	2	4	11	3	4	2	2
MG5	67	4	3	4	8	2	6	0.5	1
MG6	72	3	2	5	7	4	4	1	2
MG7	73	2	3	4	5	6	5	1	1
MG8	65	1	1	3	4	3	6	-	3
MG9	75	2	2	5	4	3	6	-	3

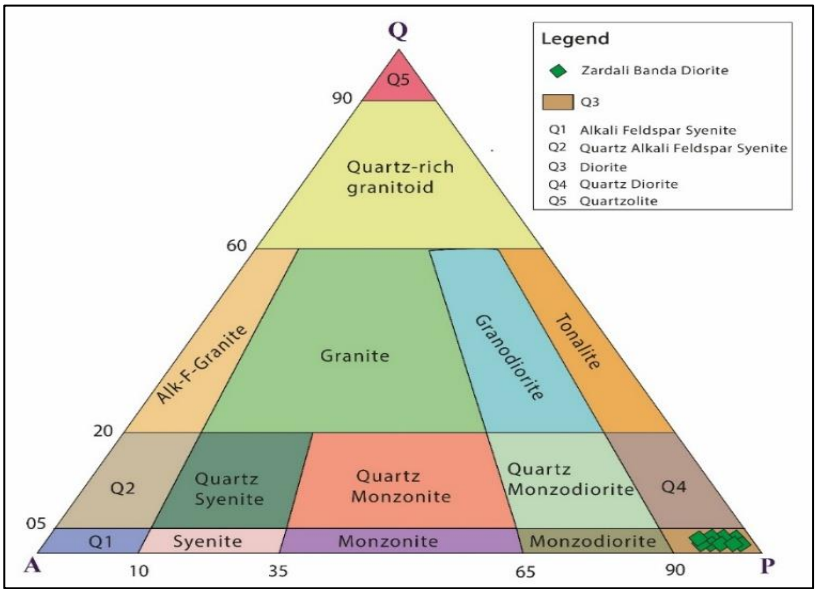

Fig. 3 Model mineralogical composition of the ZardAli Banda Diorite. (after Le Maitre (2002)).

shear zones suggest a complex history of deformation. In some areas, the rock is characterized by higher concentrations of hornblende and thread veins, often associated with the alternating shear and compacted zones (Fig. 2). These field variations influence the mechanical properties of diorite and its suitability for use as aggregate material.

3.2. LABORATORY ANALYSIS

The twenty different rock samples were collected in the field, out of twenty, nine were selected for the petrographic thin section. The rock samples were cut with the help of a rock-cutting machine and prepared as thin sections at the rock-cutting laboratory at Quaid- i-Azam University Islamabad. The study of thin sections and photomicrographs, the Nickon polarizing microscope was used at the Sedimentology laboratory of the National Center of Excellence in Geology, University of Peshawar. The geochemical analysis was executed at the Centralized Resources Laboratory, University of Peshawar. The different tests for the physical and mechanical properties are performed according to the ASTM standard tests for the coarse aggregates. The specific gravity and absorption, elongation, and flakiness index tests, Los Angeles Abrasion, soundness, Unconfined Compressive Strength (UCS), and Unconfined Tensile Strength were determined at the National Logistics Cell (NLC) Islamabad.

4. RESULTS

4.1. PETROGRAPHY

The ZardAli Banda Diorite observed thin sections are primarily composed of plagioclase, quartz, alkali feldspar (orthoclase), hornblende, clinopyroxene, orthopyroxene, and biotite, with a sufficient amount of sericite and olivine as illustrated in Figures 4a-4f. The detailed estimated percentage along with the petrographic features of each mineral are described below.

The plagioclase is the most basic mineral of diorite, having recorded percentage of 65 % to 75 % (Table 1). The plagioclase is subhedral to anhedral with certain types of twinning (Figs. 4e, 4f). The several types of sericite plagioclase were also noticed. Sericite is the common alteration product of plagioclase subjected to hydrothermal alteration (Figs. 4a, 4b, 4c). The quartz is the most prominent mineral for IUGS classification rocks. The estimated percentage of subhedral to anhedral quartz is ranges from 1 % to 4 % (Table 1, Fig. 4a). The strained quartz was also noticed during the petrographic study, with the 1st order yellow interference color showing strained conditions (Fig. 4f). The dark grey alkali

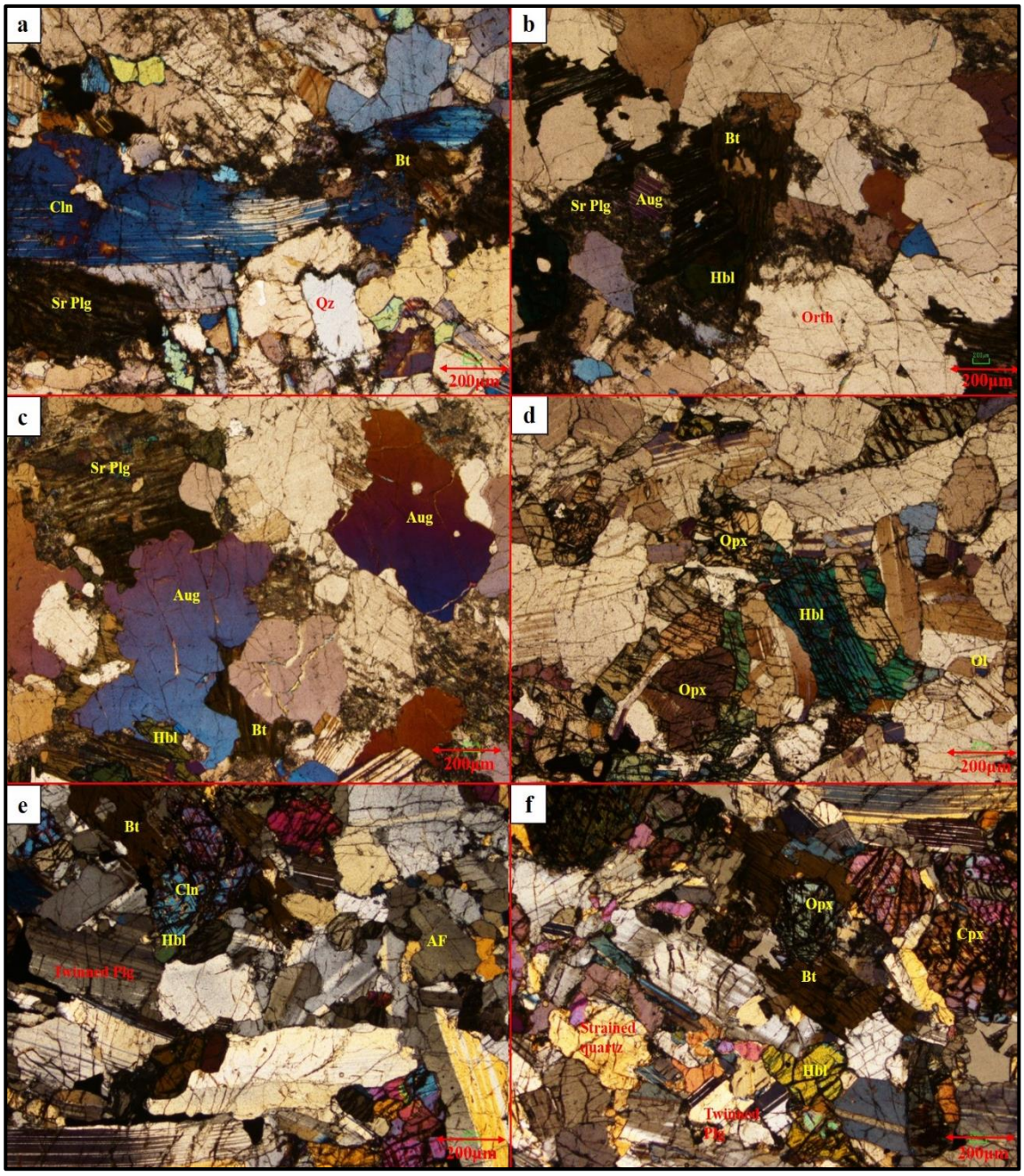

Fig. 4 Photomicrograph showing (**a**) Sericitized plagioclase, biotite, and quartz (**b**) hornblende, orthoclase, and augite (**c**) hornblende, biotite, and sericitized plagioclase (**d**) orthopyroxene, hornblende and olivine. (**e**) twinned plagioclase, clinopyroxene, and alkali feldspar (**f**) strained quartz, orthopyroxene, and twinned plagioclase. (**Key:** Plg; Plagioclase, Sr Plg; Sericitized Plagioclase, Qtz; Quartz AF; Alkali-Feldspar, Orth; Orthoclase, Bt; Biotite, Aug; Augite, Hbl; Hornblende, Cpx; Clinopyroxene, Opx; Orthopyroxene, Ol; Olivine).

feldspar color is mainly consisted of orthoclase having cleavages and a yellowish pink color observed at a thin section, ranging from 2 % to 10 % (Table 1, Fig. 4b). The well-sufficient amount greenish blue to dark green hornblende with a recorded concentration of 3 % to 6 % shows mainly associations with biotite (Table 1, Fig. 4b). The clinopyroxene with dominant minerals of augite can be seen with the amount of 4 % to 15 % having cleavages and inclusions of accessories (Table 1). The biotite flakes are the next most common mineral, having a percentage from 4 % to 6 % (Table 1, Figs. 4a, 4e, 4f). In the microscopic study, the biotite forms the continuous flow form of flakes having inclusion of orthopyroxene (Fig. 4f). The grey color orthopyroxene bulks are recorded as having concentrations of 1 % to 6 % with cleavages (Table 1, Fig. 4f). The minor amount of deep blue olivine was noticed in the petrographic investigations, ranging from 0.5 % to 2 % (Table 1, Fig. 4c). The alteration product sericite was recorded from the thin section study having a concentration of 1 % to 3 % (Table 1, Fig. 4c).

Table 2 Major oxides concentration of ZardAli Diorite.

SAMPLE	SiO_2	TiO_2	Al_2O_3	Fe_2O_3	MgO	CaO	Na_2O	K_2O	P_2O_5
MG1	59.03	0.39	22.3	6.04	0	9.2	2.15	0.62	0
MG2	58.86	0.56	22.6	6.22	0	8.66	2.32	0.78	0
MG3	57.76	0.62	23.31	6.16	0	8.45	2.89	0.81	0
MG4	57.46	0.57	24.01	6.08	0	8.2	3.11	0.57	0
MG5	56.63	0.77	23.97	6.35	0	8.27	3.27	0.74	0
MG6	56.97	0.71	22.82	6.41	0	8.97	3.24	0.88	0
MG7	58.23	0.74	21.76	6.86	0	8.33	3.19	0.89	0
MG8	58.43	0.45	22.35	6.42	0	8.46	3.12	0.77	0
MG9	57.91	0.37	23.11	6.09	0	8.93	2.98	0.61	0

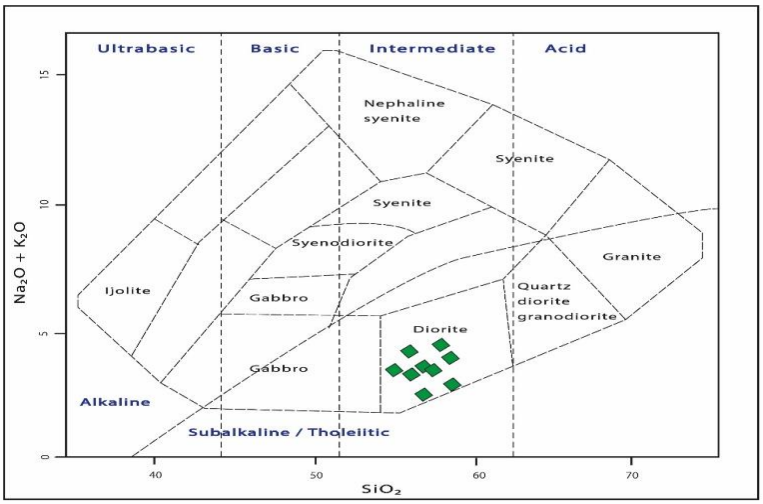

Fig. 5 Total Alkali Silica Classification for plutonic rocks (Cox et al., 1979).

4.2. GEOCHEMSITRY

The ZardAli Banda Diorite is intermediate in nature, having the SiO_2 percentage from 56.63 % to 59.03 %, followed by Al_2O_3 composition ranging from 21.76 % to 24.01 %, CaO 8.2 % to 9.2 %, Fe_2O_3 6.04 % to 6.86 %, Na_2O 2.15 % to 3.67 %, TiO_2 0.37 % to 0.77 %, K_2O 0.61 % to 0.77 % and P_2O_5 0 respectively, as illustrated in Table 2.

4.2.1. ROCKS CLASSIFICATION DIAGRAMS

The total alkali silica classification of plutonic rocks of Cox et al. (1979) suggests the diorite portion for the studied samples as shown in Figure 5.

4.2.2. MAJOR OXIDES CORRELATION

The major oxides correlation is used to determine the effect of one oxide concentration on the other oxides concentration. This analysis helps us to establish the general trend of one oxide against each other. The linear regression analysis with R^2 is listed below to understand the correlation of one oxide variations on the other major oxides as illustrated in Figures 6a-6f. The SiO_2 has an inverse relationship with Al_2O_3, K_2O, Fe_2O_3 and they indicate the fractionation of biotite during crystallization (Figs. 6c, 6d, 6e). The inverse relationship between SiO_2 and Na_2O suggests the rock differentiation process and the crystallization of silicate minerals (Fig. 6a). The positive trend line of SiO_2 vs CaO suggests the formation of calcium-rich plagioclase minerals like anorthite (Fig. 6b). The negative relationship of TiO_2 with SiO_2 shows the formation of more silica-concentrated rocks. The consumption of TiO_2 increases due to the crystallization of titanium bearing minerals in the magmatic differentiation process, as illustrated in Figure 6f.

4.3. PHYSICO-MECHANICAL PROPERTIES

4.3.1. SPECIFIC GRAVITY AND WATER ABSORPTION

The strength and quality of the aggregates can be determined from the specific gravity. The specific gravity can be determined by its mineralogical composition, which indicates the aggregates resistance to compaction (Abu Seif, 2015). The absorption is the potential study of the pores present in the rocks. The literature-recommended study shows the linear relationship between the pore spaces and absorption while showing an inverse relationship with specific gravity (Anovitz and Cole, 2015). The ZardAli Banda Diorite specific gravity ranges from 2.81gm/cm^3 to 2.85 gm/cm^3 with a mean value of 2.832 gm/cm^3 (Table 3). The ASTM limit of the specific gravity

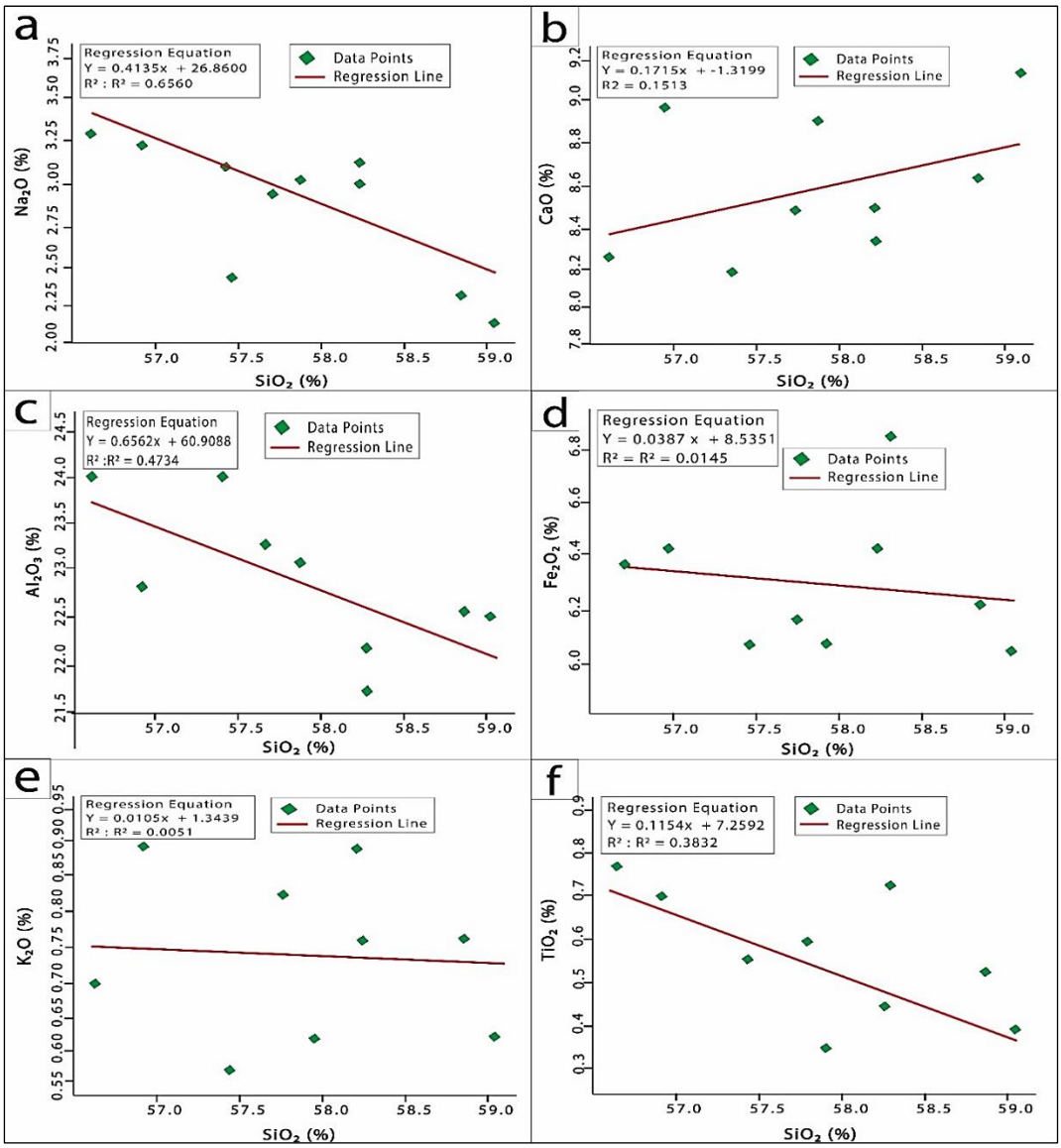

Fig. 6 Major oxides (wt.%) versus SiO_2 variations diagrams of ZardAli Banda Diorite.

(ASTM C127-12; Blyth and de Freitas, 1974) is greater than 2.5 gm/cm^3. The studied samples of diorite are within the domain of the ASTM range, and must be considered for heavy construction works.

The absorption values of ZardAli Banda Diorite fall between 0.61 % and 0.66 % with a mean of 0.627 % (Table 3). The suggested limit for absorption (ASTM C127-12) is 1 %, while Khan et al. (2024) stated that absorption up to 2 % can be used for construction works. The ZardAli Banda Diorites are within the range of (ASTM C127-12), and Khan et al. (2024) can be used as a suitable material for aggregate purposes.

4.3.2. FLAKINESS AND ELONGATION INDEX

The flakiness and elongation index is used to assess the particle shape of the aggregate. The presence of flakier and elongated materials makes the aggregate harsh and difficult to utilize. The more flakiness and elongated materials will reduce the workability and strength of the aggregates (Ponnada, 2014). The mean values of flakiness and elongation index of diorite are 4.497 % and 6.527 %, respectively (Table 3). The limits for flakiness and elongation index are 15 % (ASTM D 4791), which means that this diorite is favorable to use as construction materials.

4.3.3. LOS ANGELES ABRASION

The Los Angeles abrasion is the resistance to abrasion, grinding, and degradation of an aggregate to stress conditions. The lower value of the Los Angeles Abrasion, the higher the competency of resistance to crushing and disintegration of aggregates (Chan et al., 2023). The Los Angeles abrasion values of the diorite fall within 11.9 % to 12.45 % with a mean value of 12.58 % (Table 3). These diorite rocks are within the specified limits of ASTM C 131-06 (max. limits 40 %) to use as aggregate materials.

Table 3 Results of various Physio-mechanical analysis.

Sample No	Specific Gravity (gm/cm^3)	Abs. (%)	FI (%)	EI (%)	LAAV (%)	Soundness (%)	UCS (MPa)	UTS (MPa)
MG-1	2.84	0.63	4.52	6.71	12.01	3.3	36.88	6.12
MG-2	2.82	0.65	4.39	6.54	12.45	3.46	37.13	6.38
MG-3	2.83	0.63	4.42	6.09	12.36	3.43	36.71	5.95
MG-4	2.85	0.61	4.49	6.25	12.12	3.34	38.22	6.54
MG-5	2.84	0.62	4.56	6.45	11.9	3.29	36.96	6.17
MG-6	2.83	0.63	4.48	6.41	12.22	3.36	36.64	6.08
MG-7	2.81	0.66	4.41	6.51	12.35	3.38	35.82	5.61
MG-8	2.83	0.62	4.56	6.85	12.07	3.34	36.62	6.04
MG-9	2.85	0.6	4.65	6.94	11.95	3.32	37.25	6.47
Mean	**2.832**	**0.627**	**4.497**	**6.527**	**12.158**	**3.357**	**36.914**	**6.151**

4.3.4. SOUNDNESS

The soundness is the resistance of aggregate to environmental factors, such as weathering and erosion, wetting and drying (Okogbue and Ugwoke, 2015). The aggregates having low loss of mass in the test are considered to be more suitable in the snowfall and higher temperature zone than those having more loss of mass (Khan et al., 2024). The ASTM (C88-13) limit for the sound aggregate is 12 %, while the study samples fall in the 3.29 % to 3.46 % with a mean of 3.357 % (Table 3). This analysis suggests that diorite is the most complete package to use in construction projects associated with climatic and environmental changes.

4.3.5. UNCONFINED COMPRESSIVE STRENGTH (UCS)

Unconfined Compressive Strength refers to the maximum pressure that a rock can absorb before breaking under stress (Feng et al., 2022). UCS is widely recognized as the fundamental test to determine the mechanical strength of rocks. The samples of ZardAli Banda Diorite show strength of 35.82 MPa to 38.22 Mpa with a mean of 36.914 MPa (Table 3).

4.3.6. UNCONFINED TENSILE STRENGTH (UTS)

UTS measures the tensile strength of rocks when a load is applied at a right angle to the axis of the sample. This tensile strength is much lower than the unconfined compressive strength (Efe et al., 2021). The results of the UTS analysis range from 5.95 MPa to 6.38 MPa with a mean value of 6.151 MPa (Table 3).

4.4. DISCUSSION

4.4.1. IMPACT OF GEOCHEMICAL TREND ON PHYSICO-MECHANICAL ANALYSES

The geochemical relationships show the impact of major oxide variations on mineral crystallization and physico-mechanical properties. The inverse relationship between SiO_2 and TiO_2 suggests the crystallization of titanium-bearing minerals. These minerals are typically consumed in the formation of quartz, which enhances the diorite stability and resistance to environmental factors (Esmaeily et al., 2010). The reduction of TiO_2 is linked to the formation of silica-rich minerals having improved weathering resistance and enhanced durability (Munafo et al., 2015) as illustrated in Figure 7.

The negative relationship between SiO_2 and Al_2O_3 reflects the fractionation of anorthite plagioclase. Plagioclase contributes to moderate specific gravity (2.832 g/cm³) and low absorption percentage (0.627 %) but its higher content reduces the tensile strength because of its mineral cleavage planes, which act as potential failure points under stress (Nadaf et al., 2024; Fig. 7).

The negative relationship between SiO_2 and Fe_2O_3 suggests crystallization of ferromagnesian minerals such as hornblende, clinopyroxene, and orthopyroxene (Khedar et al., 2022). These minerals provide high mechanical strength, improving the rock's unconfined compressive strength (36.91 MPa). However, ferromagnesian minerals are more prone to weathering and oxidation, which can negatively affect long-term durability under environmental exposure (Bahurudeen et al., 2022; Fig. 7).

The positive correlation of SiO_2 with CaO is associated with the crystallization of calcium-rich plagioclase, such as anorthite ($CaAl_2Si_2O_8$). This contributes to higher compressive strength and durability due to plagioclase's high density and resistance to chemical alteration. The presence of calcium-rich plagioclase also reduces water absorption, enhancing the rock's suitability for construction in wet environments (Rashwan et al., 2019; Fig. 7).

The positive relationship with alkalis (Na_2O and K_2O) indicates the formation of alkali feldspars and quartz during late magmatic stages (Brotzu et al., 2005). These minerals are mechanically strong, contribute to low Los Angeles Abrasion Values (12.58 %), and enhance the rock's resistance to crushing. Additionally, alkali feldspars improve the rock's ability to withstand tensile stress, contributing to higher unconfined tensile strength (UTS 6.15 MPa) (Asif et al., 2024; Fig. 7).

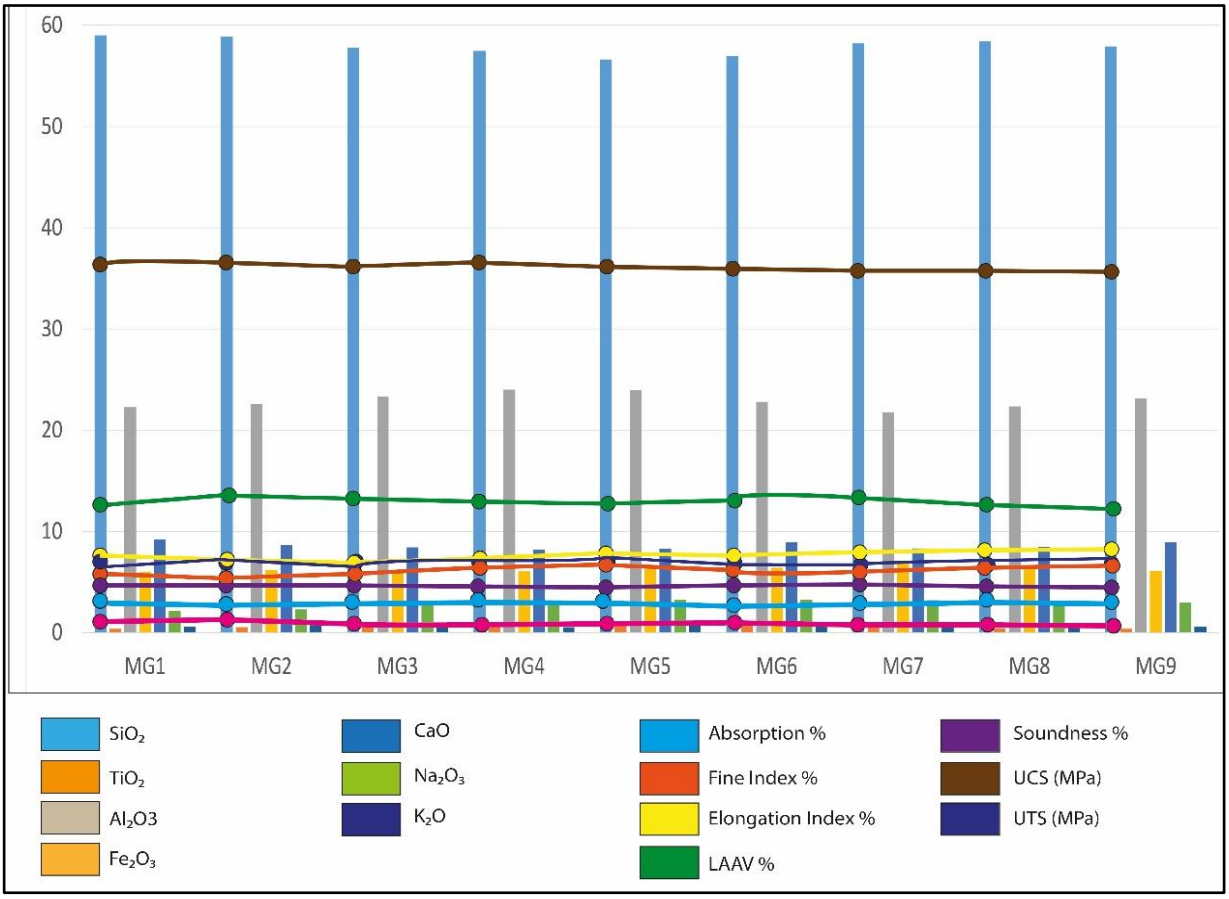

Fig. 7 Bar chart showing the relationship among the major oxides content and physico-mechanical properties of ZardAli Banda Diorite.

4.4.2. PHYSICO-MECHANICAL CORRELATION

The linear regression analysis along with R^2 is run to establish a relationship between the physico-mechanical properties to show the effects of strength analysis against each other as illustrated in Figures 8a-8w. These established relationships are plotted or compared with other published correlations by various authors. The absorption has inverse trend with specific gravity, UCS having a moderate regression line relationship (Figs. 8a, 8f). This statement has been supported by various authors including Nawaz et al. (2023), Fei et al. (2023), and Ahmad et al. (2021). The absorption has a negative relationship with the flakiness index and elongation index, as illustrated in Figures 8b and 8c. This correlation has been noted according to Naeem et al. (2014). The absorption has a positive relationship with Los Angeles Abrasion value and soundness (Figs. 8d, 8e). This relationship has been supported by Tunc and Alyamac (2019), Teymen (2019), and Mohajerani et al. (2017). The specific gravity is directly proportional to the flakiness index and elongation index (Figs. 8g, 8h). The specific gravity has an inverse relation with Los Angeles Abrasion value and soundness, while in direct relation s with UCS and UTS (Figs. 8i, 8j, 8k, 8l). The UCS and UTS have an inverse graph with Los Angeles Abrasion value and soundness (Figs. 8r, 8s, 8t). This statement has been verified by Khan et al. (2024), Asif et al. (2024) and Asif et al. (2022).

The flakiness index has a positive relationship with the UCS and UTS as shown in Figures 8t and u. This statement is against Ahmad et al. (2021). In fact, the presence of flakier materials reduces the strength because of the fracturing tendency in stress and shocks. The flakiness and elongation index have an inverse relationship between Los Angeles Abrasion Value and soundness because of the fact that flakier and elongated materials are easy to degrade and disintegrate. This statement is verified by Nweke and Okogbue (2021), while the Jaddah diorite study of Sedek Abu Seif and Sonbul (2017) shows the strong linear regression line of the flakiness and elongation index with the Los Angeles Abrasion Value (as shown in Figures 8v and w) against the ZardAli Banda Diorite for comparative analysis).

5. CONCLUSION

The petrographic, geochemical, and physico-mechanical analysis of ZardAli Banda Diorite has been investigated, leading to the following conclusion.

1. Petrographic observations show that this diorite is composed of coarse-grained texture and 8

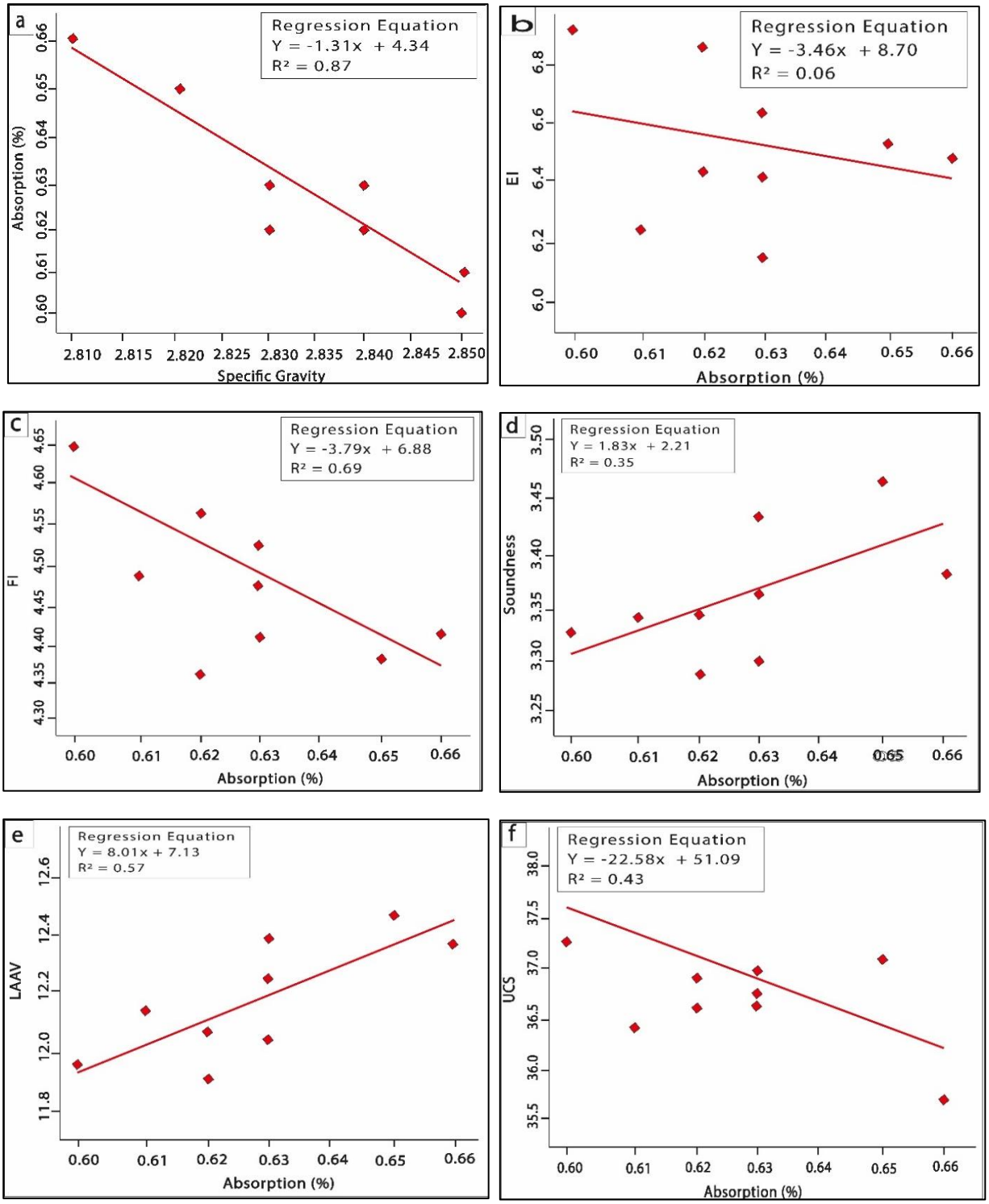

Fig. 8 Regression analysis showing (**a**) a negative trend line between specific gravity and absorption, (**b**) a positive trend line between absorption and soundness (**c**) a negative line between absorption and the Flakiness index (**d**) a positive trend line between absorption and soundness (**e**) a positive trend line between absorption and LAAV, (**f**) a negative trend line between absorption and UCS.

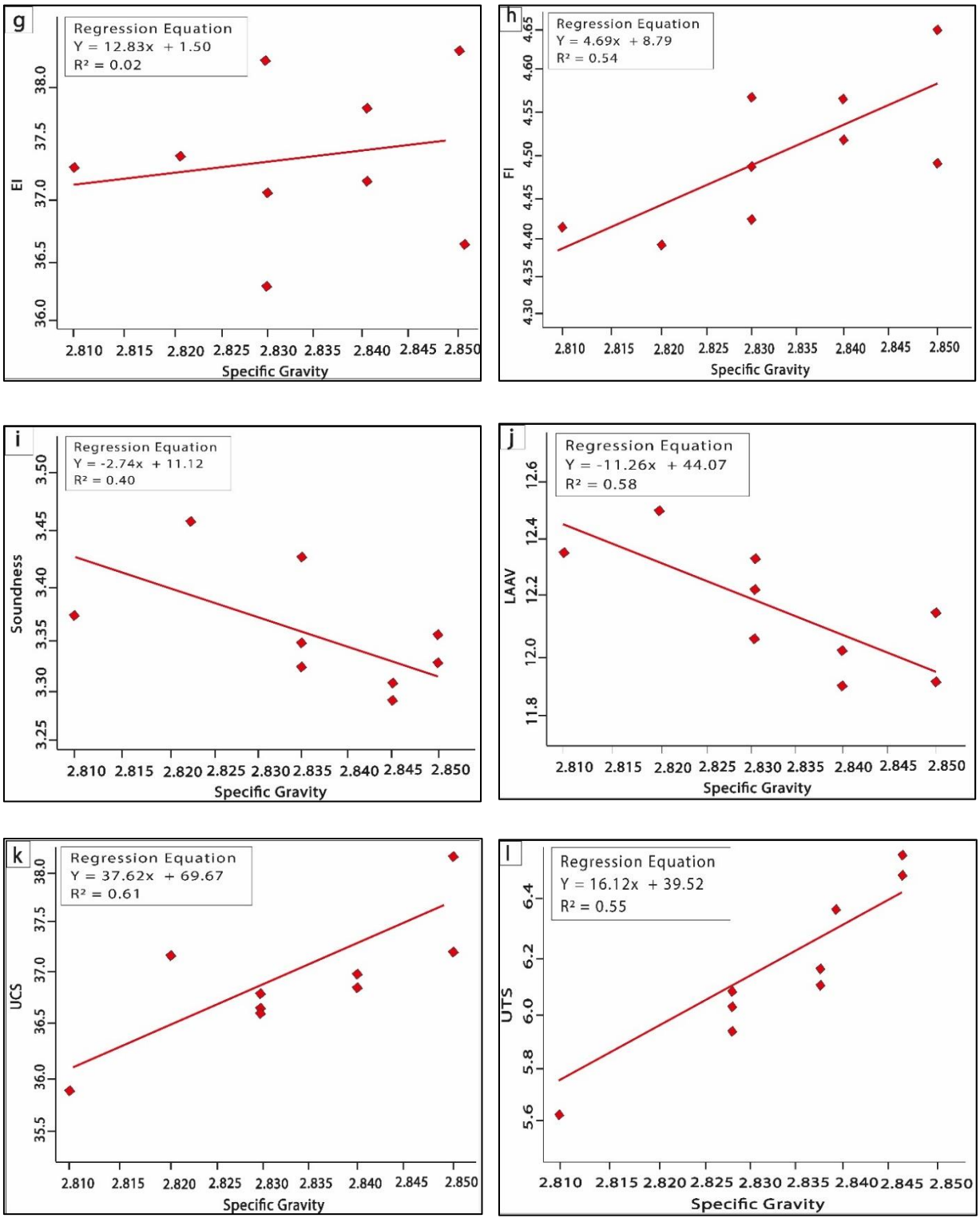

Fig. 8 (cont.) Regression analysis showing (**g**) a positive trend line between specific gravity and EI and (**h**) a positive trend line between specific gravity and FI (**i**) a negative relationship between specific gravity and soundness (**j**) a negative relationship between specific gravity and LAAV (**k**) a positive trend line between specific gravity and UCS (**l**), the corrected version should be a positive trend line between specific gravity and UTS.

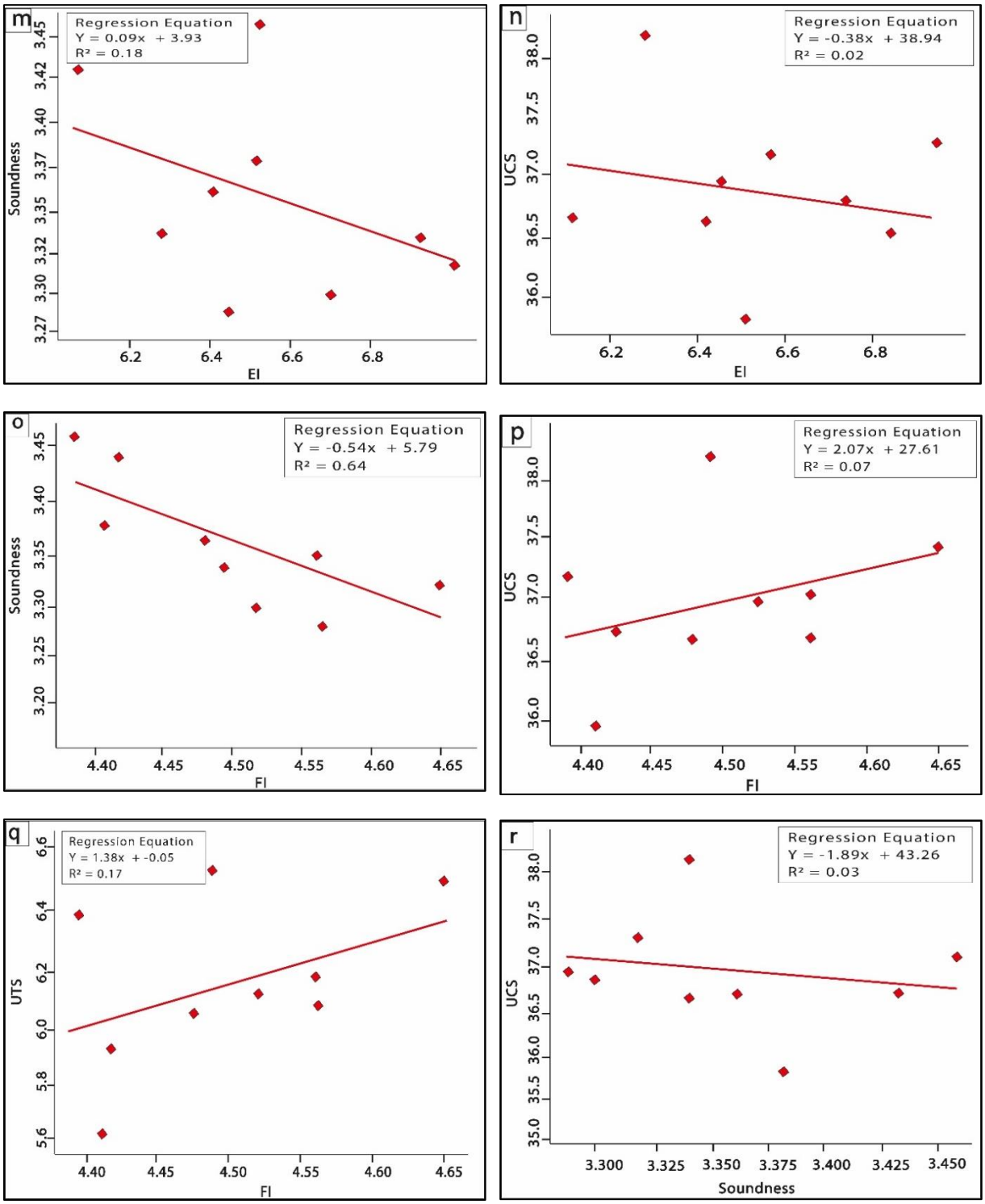

Fig. 8 (cont.) Regression analysis showing (**m**) a negative trend line between EI and soundness (**n**) a negative trend line between EI and UCS (**o**) a negative trend line between FI and soundness (**p**) a positive trend line between FI and UCS(**q**) a positive trend line between FI and UTS (**r**) a negative trend line between soundness and UCS.

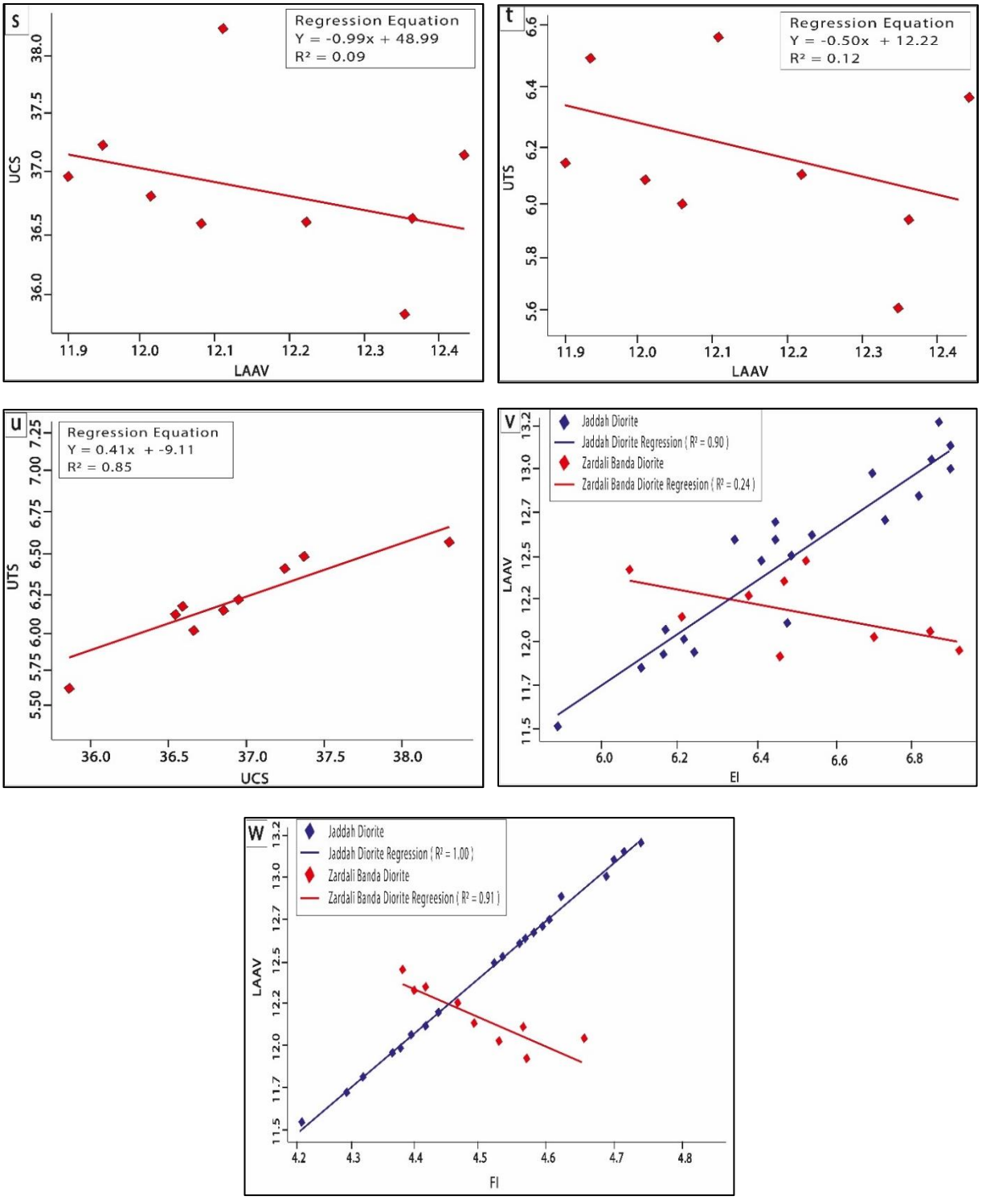

Fig. 8 (cont.) Regression analysis showing (**s**) a negative trend line between LAAV and UCS (**t**) a negative trend line between LAAV and UTS (**u**) a positive trend line between UCS and UTS (**v**) a comparative study of EI vs LAAV of ZardAli Banda Diorite and Jaddah Diorite, and (**w**) a comparative study of EI vs LAAV of ZardAli Banda Diorite and Jaddah Diorite.

interlocking patterns of plagioclase, quartz, alkali feldspar (orthoclase), hornblende, clinopyroxene, orthopyroxene, biotite, with accessory minerals of sericite and traces of olivine contributing to high mechanical strength and durability, making it suitable for aggregate applications.

2. The Geochemical composition includes SiO_2 percentages ranging from 56.63 % to 59.03 %, followed by Al_2O_3 composition ranging from 21.76 % to 24.01 %, CaO 8.2 % to 9.2 %, Fe_2O_3 6.04 % to 6.86 %, Na_2O 2.15 % to 3.67 %, TiO_2 0.37 % to 0.77 %, K_2O 0.61 % to 0.77 % and P_2O_5 0 % respectively. The moderate silica content enhances strength and weathering resistance, while the presence of calcium-rich plagioclase contributes to higher density and lower water absorption, improving durability in wet environments. The inverse correlation between SiO_2 and Fe_2O_3 suggests that ferromagnesian minerals (hornblende, pyroxenes) contribute to increased mechanical strength, making the rock resilient under stress conditions. The geochemical stability and absence of excessive alkalis or deleterious oxides indicate that the diorite is chemically stable for use in large-scale infrastructure projects.
3. The average specific gravity value of the Zard Ali Diorite is 2.832 gm/cm^3 which falls within the specified limits. The average flakiness observed in the diorite is 4.497 %, and the elongation is about 6.527 %, which is feasible to use for construction purposes. The average Los Angeles Abrasion value for the desired rock is 12.58 %, so it is suitable to use as an aggregate. The average soundness result is 3.357 %, so this diorite can be used as a coarse aggregate. The UCS value of the selected samples suggests the strength of the rock is moderately strong. The average UTS value of the diorite for selected core samples is 6.151 MPa.
4. Based on the above discussion, it is concluded that these diorites can be used as a dimension stone, and coarse aggregate for construction purposes, i.e. roads, highways, bridges, tunneling, and hydropower projects.

ACKNOWLEDGMENTS

The authors extend their appriciation to Abdullah Alrushaid Chair for Earth Science Remote Sensing Research, King Saud University, Riyadh, Saudi Arabia.

REFERENCES

Abu Seif, E.S.: 2015, Geotechnical approach to evaluate natural fine aggregates concrete strength, Sohag, Governorate, Upper Egypt. Arab. J. Geosci., 8, 9, 7565–7575.

Ahmad, I., Jan, M.Q. and Di Petro, J.A.: 2003, Age and tectonics implications of granitoid rocks from the Indian plate of Northern Pakistan. J. Virt. Explor., 11, 21–28. DOI: 10.3809/jvirtex.2003.00066

Ahmed, I., Basharat, M., Sousa, L. and Mughal, M.S.: 2021, Evaluation of building and dimension stone using physico-mechanical and petrographic properties: a case study from the Kohistan and Ladakh batholith, Northern Pakistan. Environ. Earth Sci., 80, 22, 1–17. DOI: 10.1007/s12665-021-10007-y

Anovitz, L.M. and Cole, D.R.: 2015, Characterization and analysis of porosity and pore structures. Rev. Mineral. Geochem., 80, 1, 61–164. DOI: 10.2138/rmg.2015.80.04

Asif, A.R., Islam, I., Ahmed, W., Sajid, M., Qadir, A. and Ditta, A.: 2022, Exploring the potential of Eocene carbonates through petrographic, geochemical, and geotechnical analyses for their utilization as aggregates for engineering structures. Arab. J. Geosci., 15, 11, 1105. DOI: 10.1007/s12517-022-10383-0

Asif, A.R., Sajid, M., Ahmed, W. and Nawaz, A.: 2024, Weathering effects on granitic rocks in North Pakistan: petrographic insights, strength classifications, and construction suitability. Environ. Earth Sci., 83, 11, 351. DOI: 10.1007/s12665-024-11655-6

ASTM C127-12: 2015, Standard Test Method for Specific Gravity and Water Absorption of Coarse Aggregate. ASTM International.

ASTM C131-06: 2006, Standard Test Method for Resistance to Degradation of Small-Size Coarse Aggregate by Abrasion and Impact in the Los Angeles Machine. ASTM International.

ASTM C88-13: 2013, Standard Test Method for Soundness of Aggregates by Use of Sodium Sulfate or Magnesium Sulfate. ASTM International. DOI: 10.1520/C0088-13

ASTM D4791-10: 2019, Standard Test Method for Flat Particles, Elongated Particles, or Flat and Elongated Particles in Coarse Aggregate. ASTM International. DOI: 10.1520/D4791-10

Bahurudeen, A., Dhanya, B. and Santhanam, M.: 2022, Concrete as in artificial rock: Mineralogy of aggregates revisited. Indian Concr. J., 96, 8, 5-36

Brotzu, P., Melluso, L., d'Amelio, F. and Lustrino, M.: 2005, Potassic dykes and intrusions of the Serra do Mar Igneous Province (SE Brazil). In: Comin-Chiaramonti, P. and Gomes, C.B. (eds.), Mesozoic to Cenozoic Alkaline Magmatism in the Brazilian Platform. São Paulo, Edusp/Fapesp, 443–472.

Cox, K.G., Bell, J.D. and Pankhurst, R.J.: 1979, The use of isotopes in petrology. In: The interpretation of igneous rocks. Springer, Dordrecht. DOI: 10.1007/978-94-017-3373-1_15

De la Roche, H., Leterrier, J., Grandclaude, P. and Marchal, M.: 1980, A classification of volcanic and plutonic rocks using R1-R2 diagrams and major element analyses–Its relationships with current nomenclature. Chem. Geol., 29, 183–210. DOI: 10.1016/0009-2541(80)90020-0

Efe, T., Demirdag, S., Tufekci, K., Sengun, N. and Altindag, R.: 2021, Estimating the direct tensile strength of rocks from indirect tests. Arab. J. Geosci., 14, 1–23. DOI: 10.1007/s12517-021-07539-9

Esmaeily, D., Rahimpour-Bonab, H., Esna-Ashari, A. and Kananian, A.: 2010, Petrography and geochemistry of the Jajarm Karst Bauxite Ore Deposit, NE Iran: Implications for source rock material and ore genesis. Turk. J. Earth Sci., 19, 2, 267–284. DOI: 10.3906/yer-0806-15

Eyal, Y., Eyal, M., Litvinovsky, B., Jahn, B. M., Calvo, R., and Golan, T.: 2019, The evolution of the Neoproterozoic Elat Metamorphic Complex, northernmost Arabian-Nubian Shield: Island arc to syncollisional stage and post-collisional magmatism. Precambrian Res., 320, 137–170. DOI: 10.1016/j.precamres.2018.10.003

Fei, L., Hinderer, M. and Hornung, J.: 2023, Paleo-weathering of different basement rocks along a first-order nonconformity-case study at the post-Variscan nonconformity (Germany). Catena, 227, 107070. DOI: 10.1016/j.catena.2023.107070

Feng, Q., Jin, J., Zhang, S., Liu, W., Yang, X. and Li, W.: 2022, Study on a damage model and uniaxial compression simulation method of frozen–thawed rock. Rock Mech. Rock Eng., 55, 6, 1–25. DOI: 10.1007/s00603-021-02645-2

Gibbons, A.D., Zahirovic, S., Müller, R.D., Whittaker, J.M. and Yatheesh, V.: 2015. A tectonic model reconciling evidence for the collisions between India, Eurasia and intra-oceanic arcs of the central-eastern Tethys. Gondwana Res., 28, 2, 451–492. DOI: 10.1016/j.gr.2015.01.001

Heuberger, S.: 2004, Kinematics of the Karakoram-Kohistan suture zone, Chitral, NW Pakistan. Doctoral dissertation, ETH Zurich.

Jan, M.Q.: 1990, Geochemistry of amphibolites from the southern part of the Kohistan arc, N. Pakistan. Mineral. Mag., 52, 365, 147-159. DOI: 10.1180/minmag.1988.052.365.02

Kausar, A.B., Yamamoto, H., Kubo, K., Takahashi, Y., Mikoshiba, M.U. and Rehman, H.U.: 2004, Trace and Rare-Earth Elements distribution patterns of rocks of Chilas Complex and Kamila Amphibolites, Kohistan Arc, North Pakistan. Himal. J. Sci., 2, 4, 173–174. DOI: 10.3126/hjs.v2i4.859

Khan, E.U., Saleem, M., Sajjad, S.M.W., Ahmad, S.M. and Khan, A.: 2024, Petrographic, mechanical and aggregate analysis of Jurassic Samana Suk Formation Kahi Section, Nizampur Basin, Pakistan. Iran J. Earth Sci., 16, 3, 1–11. DOI: 10.57647/j.ijes.2024.1603.16

Khan, S.D., Walker, D.J., Hall, S.A., Burke, K.C., Shah, M.T. and Stockli, L.: 2009, Did the Kohistan-Ladakh island arc collide first with India? Geol. Soc. Am. Bull., 121, 3-4, 366–384. DOI: 10.1130/B26348.1

Khedr, M.Z., Takazawa, E., Arai, S., Stern, R.J., Morishita, T. and El-Awady, A.: 2022, Styles of Fe–Ti–V ore deposits in the Neoproterozoic layered mafic-ultramafic intrusions, south Eastern Desert of Egypt: Evidence for fractional crystallization of V-rich melts. J. Afr. Earth Sci, 194, 104620. DOI: 10.1016/j.jafrearsci.2022.104620

Le Maitre, R.W. (Ed.): 2002, Igneous rock: a classification and glossary of terms, 2nd Edition. Cambridge University Press. DOI: 10.1017/CBO9780511535581

Mohajerani, A., Nguyen, B.T., Tanriverdi, Y. and Chandrawanka, K.: 2017, A new practical method for determining the LA abrasion value for aggregates. Soils Found., 57, 5, 840–848. DOI: 10.1016/j.sandf.2017.08.013

Munafò, P., Goffredo, G.B. and Quagliarini, E.: 2015, TiO_2-based nanocoatings for preserving architectural stone surfaces: An overview. Constr. Build. Mater., 84, 201–218. DOI: 10.1016/j.conbuildmat.2015.02.083

Nadaf, M.B., Maralapalle, V., Zende, A.A. and Momin, A.I.: 2024, Mineralogical composition and strength characteristics of granite rocks. Sadhana, 49, 4, 1–22. DOI: 10.1007/s12046-024-02635-4

Naeem, M., Khalid, P., Sanaullah, M. and ud Din, Z.: 2014, Physio-mechanical and aggregate properties of limestones from Pakistan. Acta Geod. Geophys., 49, 3, 369–380. DOI: 10.1007/s40328-014-0054-8

Nakazawa, C., Rehman, H.U., Yamamoto, H. and Zafar, T.: 2020, Zirconium in rutile thermometry from garnet granulites of the Jijal complex of Kohistan arc, NW Himalaya. J. Mineral. Petrol. Sci, 115, 2, 152–161. DOI: 10.2465/jmps.191226

Nawaz, M., Ahmed, W., Yasir, M., Islam, I., Janjuhah, HT., Kontakiotis, G. and Stouraiti, C.: 2023, Petrographic and geotechnical features of Dir Volcanics as dimension stone, Upper Dir, North Pakistan. Geosci. J., 13, 8, 224. DOI: 10.3390/geosciences13080224

Nweke, O.M., and Okogbue, C.O.: 2021, Geotechnical evaluation of the quality and durability of argillites from Abakaliki Metropolis (Southeastern Nigeria) as road aggregates. Arab. J. Geosci., 14, 1–24. DOI: 10.1007/s12517-021-08613-y

Okogbue, C.O. and Ugwoke, T.A.: 2015, Influence of petrogenesis on suitability of some pelitic rocks as construction aggregates in South-eastern Nigeria. Geotech. Geol. Eng., 33, 1395–1407. DOI: 10.1007/s10706-015-9908-2

Petterson, M.G.: 2019, The plutonic crust of Kohistan and volcanic crust of Kohistan–Ladakh, north Pakistan/India: lessons learned for deep and shallow arc processes. Geol. Soc. Spec. Publ., 483, 1, 123–164. DOI: 10.1144/SP483.4

Petterson, M.G.: 2010, A review of the geology and tectonics of the Kohistan island arc, north Pakistan. Geol. Soc. Spec. Publ., 338, 1, 287–327. DOI: 10.1144/SP338.14

Ponnada, M.R.: 2014, Combined effect of flaky and elongated aggregates on strength and workability of concrete. Int. J. Struct. Eng., 5, 4, 314–325. DOI: 10.1504/IJSTRUCTE.2014.065915

Rehman, H.U., Khan, T., Lee, H.Y., Chung, S.L., Jan, M.Q., Zafar, T. and Murata, M.: 2021, Petrogenetic source and tectonic evolution of the Neoproterozoic Nagar Parkar Igneous Complex granitoids: Evidence from zircon Hf isotope and trace element geochemistry. Precambrian Res., 354, 106047. DOI: 10.1016/j.precamres.2020.106047

Richards, J.P.: 2015, Tectonic, magmatic, and metallogenic evolution of the Tethyan orogen: From subduction to collision. Ore Geol. Rev., 70, 323–345. DOI: 10.1016/j.oregeorev.2014.11.009

Searle, M.P.: 2019, Timing of subduction initiation, arc formation, ophiolite obduction and India–Asia collision in the Himalaya. Geol. Soc. Spec. Publ., 483, 1, 19–37. DOI: 10.1144/SP483

Sedek Abu Seif, E.S. and Sonbul, A.R.: 2017, Engineering properties of concrete made with crushed aggregate of diorite, Jeddah, Saudi Arabia. Acta Montan. Slovaca, 22, 3.

Strzałkowski, P., Duchnowska, M., Kaźmierczak, U., Bakalarz, A., Wolny, M., Karwowski, P. and Stępień, T.: 2021, Evaluation of the structure and geometric properties of crushed igneous rock aggregates. Materials, 14, 23, 7202. DOI: 10.3390/ma14237202

Teymen, A.: 2019, Estimation of Los Angeles abrasion resistance of igneous rocks from mechanical aggregate properties. Bull. Eng. Geol. Environ., 78, 837–846. DOI: 10.1007/s10064-017-1134-0

Treloar, P.J., Rex, D.C., Guise, P.G., Coward, M.P., Searle, M.P., Windley, B.F. and Luff, I.W.: 1989, K-Ar and Ar-Ar geochronology of the Himalayan collision in NW Pakistan: Constraints on the timing of suturing, deformation, metamorphism and uplift. Tectonics, 8, 4, 881–909. DOI: 10.1029/TC008i004p00881

Tunc, E.T. and Alyamac, K.E.: 2019, A preliminary estimation method of Los Angeles abrasion value of concrete aggregates. Constr. Build. Mater., 222, 437–446. DOI: 10.1016/j.conbuildmat.2019.06.176

Ullah, Z., Khan, A., Faisal, S., Zafar, T., Li, H. and Farhan, M.: 2022, Petrogenesis of peridotites in the Dargai Complex ophiolite, Indus Suture Zone, Northern Pakistan: Implications for two stages of melting, depletion, and enrichment of the Neo-Tethyan mantle. Lithos, 426, 106798.
DOI: 10. 1016/j.lithos.2022.106798

Ullah, Z., Li, H., Khan, A., Faisal, S., Dilek, Y., Förster, M.W. and Hussain, S.A.: 2023, Mineralogy and PGE geochemistry of chromitites and peridotites of the sapat complex in the indus suture zone, northern Pakistan: implications for magmatic processes in the supra-subduction zone. Int. Geol. Rev., 65, 10, 1719–1744. DOI: 10.1080/00206814.2022.2106519

Ullah, Z., Li, J.W., Robinson, P.T., Wu, W.W., Khan, A., Dac, N.X. and Adam, M.M.A.: 2020a, Mineralogy and geochemistry of peridotites and chromitites in the Jijal Complex ophiolite along the Main Mantle Thrust (MMT or Indus Suture Zone) North Pakistan. Lithos, 366, 105566. DOI: 10.1016/j.lithos.2020.105566

Ullah, Z., Shah, M.T., Siddiqui, R.H., Lian, D.Y. and Khan, A.: 2020b, Petrochemistry of high-Cr and high-Al chromitites occurrences of dargai complex along indus suture zone, northern Pakistan. Episodes, 43, 2, 689–709. DOI: 10.18814/epiiugs/2020/020002

Varghese, P.C.: 2011, Engineering geology for civil engineers. PHI Learning Pvt. Ltd., 264 pp.

Zafar, T., Leng, C.B., Mahar, M.A., Alam, M., Zhang, X.C., Chen, W.T. and Rehman, S.U.: 2020b, Petrogenesis, platinum-group element geochemistry and geodynamic evolution of the Cretaceous Chilas gabbros, Kohistan island arc, NE Pakistan. Lithos, 372, 105691. DOI: 10.1016/j.lithos.2020.105691

Zafar, T., Leng, C.B., Mahar, M.A., Rehman, H.U., Zhang, X.C., Chen, W.T., Alam, M. and Rehman, S.U.: 2021, Reply to the comment on Zafar et al., 2020:" Petrogenesis, platinum-group element geochemistry and geodynamic evolution of Cretaceous Chilas gabbros, Kohistan island arc, NE Pakistan" by Hussain et al., 2021. Lithos, 398, 106298.
DOI: 10.1016/j.lithos.2021.106298

Zafar, T., Leng, C.B., Zhang, X.C. and Rehman, H.U.: 2019a, Geochemical attributes of magmatic apatite in the Kukaazi granite from western Kunlun orogenic belt, NW China: Implications for granite petrogenesis and Pb-Zn (-Cu-W) mineralization. J. Geochem. Explor., 204, 256–269.
DOI: 10.1016/j.gexplo.2019.06.005

Zafar, T., Mahar, M.A., Rehman, H.U., Riaz, M., Latif, K., Oyebamiji, A. and Naeem, M.: 2019b, Geochemical and petrological characteristics of xenoliths in Mansehra Granite, NW Himalaya, Pakistan: implications for petrogenesis and tectonic settings. Episodes, 42, 4, 263–285.
DOI: 10.18814/epiiugs/2019/019022

Zafar, T., Rehman, H.U., Lutfi, W., Ullah, Z., Nouri, F., Sepidbar, F. and Rehman, S.U.: 2023, Petrogenetic, geochemical, and geochronological constraints on magmatic evolution of the Chilas Complex gabbros, Kohistan arc, NW Himalaya. Geol. J., 58, 4, 1401–1427. DOI: 10.1002/gj.4665

Zafar, T., Rehman, H.U., Mahar, M.A., Alam, M., Oyebamiji, A., Rehman, S.U. and Leng, C.B.: 2020a, A critical review on petrogenetic, metallogenic and geodynamic implications of granitic rocks exposed in north and east China: New insights from apatite geochemistry. J. Geodyn., 136.
DOI: 10.1016/j.jog.2020.101723

Zafar, T., Song, S., Rehman, H.U., Gamaleldien, H., Oyebamiji, A., Ullah, Z., Jadoon, U.F., Farhan, M., Khedr, M.Z., Bhat, I.M., Sepidbar, F., Nouri, F., Hussain, A., Hussain, Z. and Sami, M.: 2025, Retrieving petrogenetic source, compositional diversity and tectono-magmatic scenario of Tethyan sediment-derived magmatic flare-up: A tale from petrochemical and multi-isotopic (Sr–Nd–B–Hf) systematics. Gondwana Res., 141, 164–179.
DOI: 10.1016/j.gr.2025.02.013

Zafar, T., Ur Rehman, H., Maqbool Bhat, I., Ullah, Z., Farhan, M., Oyebamiji, A. and Sami, M.: 2024, Exploring the tectono-magmatic evolution of intraoceanic fore-arc setting during subduction initiation: perspectives from trace and platinum group element systematics of the Jijal ultramafic arc system, NE Pakistan. Int. Geol. Rev., 1–25.
DOI: 10.1080/00206814.2024.2318573